Journal of Water Process Engineering 33 (2020) 101019

Contents lists available at ScienceDirect

Journal of Water Process Engineering

journal homepage: www.elsevier.com/locate/jwpe

Addition of biochar into activated sludge improves removal of antibiotic ciprofloxacin

Do Gun Kim[a], Donggeon Choi[a], Seungyong Cheon[a], Seok-Oh Ko[a], Seoktae Kang[b], Seungdae Oh[a,*]

[a] Department of Civil Engineering, Kyung Hee University, Yonggin 17104, Republic of Korea
[b] Department of Civil and Environmental Engineering, Korea Advanced Institute of Science and Technology (KAIST), Daejeon 34141, Republic of Korea

ARTICLE INFO

Keywords:
Biochar
Ciprofloxacin
Activated sludge
Adsorption
Wastewater treatment

ABSTRACT

This study evaluated the effectiveness of treating a ciprofloxacin (CIP)-containing waste stream by activated sludge dosed with apple-tree-derived biochar (AB). AB was dosed to activated sludge-inoculated bioreactors with varied AB volume ratios (10 %, 20 %, and 40 % of AB to the total volume). The AB-dosed bioreactors were operated by feeding by 1 mg L^{-1} of CIP. At steady state, the AB-dosed bioreactors achieved significantly enhanced CIP removal (up to 94 %) and the removal efficiency was positively correlated with the AB volume ratio, suggesting the key role of AB on controlling the removal efficiency of AB. The CIP removals occurring in the bioreactors at steady state were largely through adsorption to AB. This work further carried out systematic assessment on the adsorption kinetics, isotherm, and characteristics of CIP on AB in variable environmental conditions. CIP adsorption onto AB was controlled by diffusion in macropores, π-π electron-donor-acceptor interactions, and electrostatic attraction. Our results suggested that hardwood-derived biochar may be a promising bio-waste additive for improving micropollutant removals in activated sludge processes, which has implications on further devising a simple and cost-effective treatment option for antibiotics-bearing waste streams.

1. Introduction

Ciprofloxacin (CIP) is a second-generation antibiotic fluoroquinolone that has been widely used for several decades. CIP interferes with bacterial DNA replication and transcription by inhibiting DNA gyrase and topoisomerase [1]. It is one of the most commonly prescribed fluoroquinolone antibiotics for various infections (e.g., skin, urinary, respiratory, and gastrointestinal tract) due to broad-spectrum antibacterial activity against Gram-negative and -positive bacteria [2]. Extensive use in clinical and domestic settings has led to the widespread occurrence of CIP in both natural and engineered water environments. CIP occurs at substantially high concentrations in waste streams associated with hospitals and pharmaceutical manufacturers. In particular, up to 31 mg L^{-1} of CIP was detected in pharmaceutical wastewater and 2.5–6.5 mg L^{-1} was measured in surface water samples of lakes and rivers associated with impacts of drug manufacturers [3]. CIP can cause mortality and genotoxicity even at a few micrograms per liter for various organisms, including primary producers (e.g., freshwater cyanobacteria and plants) essential for the function and resilience of aquatic ecosystems [4,5]. A substantial body of literature suggests that CIP carries toxicological consequences at concentrations detectable in a variety of environments.

The majority of CIP is likely released in urban waste streams through sewage disposal due to use in clinical and household environments (e.g., toilet wastewater can exhibit high levels of CIP excreted in urine and feces) [6]. Wastewater treatment plants (WWTPs) are tasked with controlling the transport of CIP to reduce ecological risks, but removal rates in conventional activated sludge processes (CASP) and anaerobic sludge processes vary greatly (20–95 %) across different WWTPs, suggesting unpredictable, if not unsatisfactory, CIP control [6,7]. Full-scale membrane bioreactors exhibit higher removal rates (73 % on average) compared with those of CASP [8]. Several organisms (e.g., bacteria, fungi, and microalgae) are capable of metabolizing CIP [9–11]. A *Bradyrhizobium* isolate originating from activated sludge (AS) achieved 70 % removal via co-metabolic pathways at environmentally relevant levels of CIP [11], implying a potential use as an auxiliary source for bioaugmentation on CIP-bearing waste streams. However, biological degradation alone using pure or mixed cultures usually takes several days, making such means less feasible in full-scale WWTPs with relatively brief- hydraulic retention times, requiring other treatment alternatives to CASP for effective control.

Wastewater treatment processes capable of reliably eliminating

* Corresponding author at: Department of Civil Engineering, Kyung Hee University, 1732 Deogyeong-daero, Giheung-gu, Yongin-si, Gyeonggi-do, 17104, Republic of Korea.
E-mail address: soh@khu.ac.kr (S. Oh).

https://doi.org/10.1016/j.jwpe.2019.101019
Received 24 August 2019; Received in revised form 19 October 2019; Accepted 21 October 2019

micropollutants (e.g., pharmaceuticals and personal care products, including CIP) as well as conventional contaminant targets have yet to be developed. Micropollutant-removal alternatives to CASP include, but are not limited to, coagulation-flocculation, activated-carbon adsorption, ozonation and advanced oxidation, membrane, and attached-growth treatment [12]. Among others, micropollutant adsorption treatment using activated carbon (AC) has become one of the commonly used and effective treatment options for full scale tertiary treatment plants [13]. A granular activated carbon process was found to remove more than 60 % of CIP from wastewaters [14]. The adsorption process can be located after the secondary effluent as a post-polishing treatment or AC can be directly dosed into activated sludge processes [15]. Although AC exhibits demonstrated adsorption capacities for diverse classes of micropollutants, its massive use may cause environmental consequences, since it requires highly demanding thermal energy for activation and emits greenhouse gas while typically produced from nonrenewable coal [13].

Biochar is a carbonaceous material that can be produced from pyrolysis (thermal degradation without oxygen) of a wide range of biomass (e.g., wood, rice straw, and bamboo) [16]. While AC production is expensive and highly energy-demanding, the use of biochar may be cost-effective and environment-friendly (e.g., sequestering carbon and valorizing organic waste) [13]. Various types of biochar have been tested for pollutants adsorption, including antibiotics, metals, and industrial chemicals [17–19]. In addition to the adsorption capacity, recent research has explored the capabilities of biochar as a microbial carrier due to its large porosity and surface area [16]. Hence, this study aimed to evaluate the technical feasibility of mitigating CIP by direct dosage of biochar to AS. To test the effects of biochar, AS-inoculated reactors were dosed with biochar at different amounts. The CIP removal and other essential functions (e.g., organic matter removal and biomass yield) of biochar-dosed reactors were monitored from reactor start-up to quasi-steady state and compared with a control AS reactor without biochar. This present study also attempted to identify the removal routes (e.g., physicochemical and biological) of CIP in biochar-dosed AS reactors and critically evaluated physicochemical mechanisms controlling the fate of CIP. The results of this work have implications on expanding current wastewater treatment options for micropollutant removal.

2. Materials and methods

2.1. Establishment of bioreactors

AS was taken from an aerobic tank of a local municipal WWTP. The AS sample was washed twice with phosphate-buffered saline (PBS, pH 7.4). Four one liter laboratory bioreactors were inoculated with AS (3 g L^{-1} volatile suspended solids [VSS]). The four reactors were filled with a range of biochar volume ratios: 0 %, 10 %, 20 %, and 40 % of total working volume. The filling ratios were comparable to a typical range (e.g., up to 70 %) of microbial carriers used in many biocarrier reactors [20], as the effects of biochar as a microbial carrier as well as an adsorbent were to be examined in this study. The apple tree biochar (AB) made from *Malus pumila* was purchased from a local manufacturer (Yougi Industry Co., Ltd., Korea). The purchased biochar was sieved by particle size between 4.8–6.4 mm, washed twice with deionized water (DIW) to remove dirt debris and dried in the oven at 105 °C for 12 h. The bulk density of AB was 0.15 ± 0.04 g mL^{-1} and the AB dosage corresponding to the 10 %, 20 %, and 40 % AB filling ratio was 1.6, 3.7, and 9.8 g mL^{-1}, respectively. All reactors consisted of an air diffuser connected to an air pump to maintain consistent dissolved oxygen. The feed was prepared with a composition similar to ElNaker et al. [21] containing 2,100 mg L^{-1} glucose, 65.8 mg L^{-1} K_2HPO_4, 43.7 mg L^{-1} KH_2PO_4, 800 mg L^{-1} NH_4Cl, 53 mg L^{-1} $CaCl_2$, 270 mg L^{-1} $MgSO_4{\cdot}7H_2O$, 9.8 mg L^{-1} $FeSO_4{\cdot}7H_2O$, and 10 ml of trace mineral solution (0.35 mg L^{-1} $ZnSO_4{\cdot}7H_2O$, 0.21 mg L^{-1} $MnSO_4{\cdot}H_2O$, 2.1 mg L^{-1} H_3BO_3, 2 mg L^{-1} $CoCl_2{\cdot}6H_2O$, 0.07 mg L^{-1} $CuCl_2{\cdot}2H_2O$, 0.14 mg L^{-1} $NiSO_4{\cdot}6H_2O$, and 0.21 mg L^{-1} $Na_2MoO_4{\cdot}2H_2O$). The chemical oxygen demand (COD) value of the feed was 2 g L^{-1}. The feed also consisted of 1 mg L^{-1} of CIP. All reactors were developed by feeding the synthetic wastewater feed twice a week (3.5 days of one cycle duration) as described previously by Oh and Choi [22]. At the end of each cycle, half of the mixed-culture suspension was discarded and replaced with an equal volume of fresh synthetic wastewater. The reactors were maintained with an organic loading rate of 0.2 kg of COD m^{-3} day^{-1}, seven days of solid retention time, and 3–4 mg L^{-1} of dissolved oxygen, comparable to those of conventional activated sludge processes.

2.2. Analysis of CIP adsorption kinetics

Kinetic experiments for CIP adsorption to AB were performed in separate bottles with the same condition of the bioreactor operation, excluding biomass. Glass bottles were filled with 200 mL synthetic feed containing 1 mg L^{-1} CIP. 1.6, 3.7, and 9.8 g L^{-1} of pre-treated AB was put into the bottles, which were equivalent to the volumetric AB ration of 10, 20, and 40 % as in the bioreactors, respectively. The adsorption of CIP to AS was investigated in the same manner where only AB was replaced with AS, at a dose of 3 g VSS L^{-1} as initially inoculated for the bioreactor set-up. Time course CIP adsorption data were fitted to pseudo-first-order, pseudo-second-order and Weber and Morris intra-particle diffusion models [23], as shown in Eqs. (1)–(3), respectively:

$$\frac{dq}{dt} = k_{a1}(q_e - q) \tag{1}$$

$$\frac{dq}{dt} = k_{a2}(q_e - q)^2 \tag{2}$$

$$q_t = k_{diff}{\cdot}t^{1/2} + c \tag{3}$$

where, q (mg g^{-1}) is the adsorbed CIP amount at time t, q_e (mg g^{-1}) is the equilibrium adsorption amount of CIP, k_{a1} (min^{-1}) is the pseudo-first-order adsorption rate constant, k_{a2} (mg g^{-1} min^{-1}) is the pseudo-second-order adsorption rate constant, k_{diff} (mg g^{-1} $min^{-1/2}$) is the intra-particle diffusion rate constant, and c is a constant representing the thickness of boundary layer.

2.3. Analysis of CIP adsorption isotherm

Isotherm experiments of CIP to AB were carried out using 0.1 g of AB in 50 mL glass vials containing 40 mL of DIW. CIP concentrations established in the vials ranged from 2.5–250 mg L^{-1}. The vials were shaken at 150 rpm for 24 h at room temperature (RT). Similar experiments were performed using AS (instead of AB) at a dose of 0.1 g dry weight and at CIP concentrations of 0.5–21.3 mg L^{-1}. Experimental data were fitted to the Langmuir, Freundlich, Sips and Dubinin–Kaganer–Radushkevich isotherm models as given in Eqs. (4)–(7) [24]:

$$q_e = q_{\max,L}\frac{K_L C_e}{1 + K_L C_e} \tag{4}$$

$$q_e = K_F C_e^{1/n} \tag{5}$$

$$q_e = q_{\max,S}\frac{(K_S C_e)^{\beta}}{1 + (K_S C_e)^{\beta}} \tag{6}$$

$$q_e = q_S \exp(-k_{ad}\varepsilon^2) \tag{7}$$

where, q_e is the equilibrium adsorption amount (mg g^{-1}), $q_{max,L}$ is the maximum adsorption capacity of the Langmuir isotherm (mg g^{-1}), C_e is the equilibrium adsorbate concentration (mg L^{-1}), K_L is the Langmuir isotherm constant (L mg^{-1}), K_F is the Freundlich isotherm constant related to adsorption capacity (mg g^{-1} [L mg^{-1}]$^{1/n}$), $1/n$ is a dimensionless factor that measures the adsorption intensity or surface

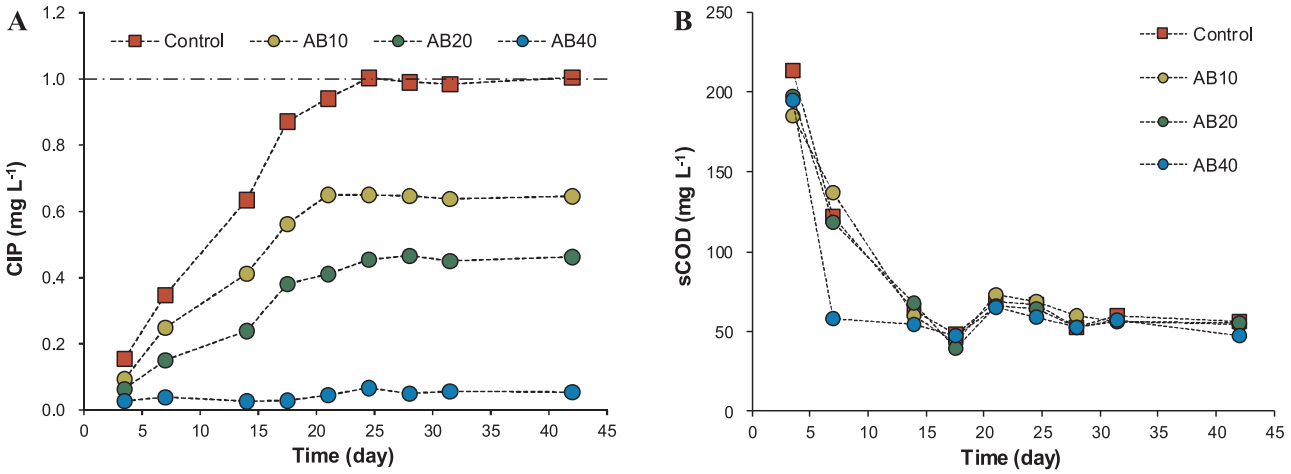

Fig. 1. (A) CIP concentrations in effluents from the four bioreactors. The dash-dot line represents the influent CIP concentration. (B) sCOD concentrations in effluents from the four reactors. The CIP and COD concentrations were measured at the end of each feeding cycle (3.5 days of a cycle duration). Markers represent the mean value of triplicate measurements with < 5 % of standard deviation from the mean. The COD removal rates at steady state (days 24.5–42) among the four reactors did not differ significantly ($P > 0.05$ by Mann-Whitney U test).

heterogeneity, $q_{max,S}$ is the maximum adsorption capacity of the Sips isotherm (mg g^{-1}), K_S (L $mmol^{-1}$) is the Sips isotherm model constant, β is the Sips isotherm model exponent related to surface heterogeneity, q_S is the saturation capacity of Dubinin–Kaganer–Radushkevich isotherm (mg g^{-1}), and k_{ad} is Dubinin–Kaganer–Radushkevich isotherm constant related to adsorption energy (mol^2 kJ^{-2}). The term ε is the Polanyi potential defined as in Eq. (8) and the free energy of adsorption (E, kJ mol^{-1}) was calculated using Eq. (9):

$$\varepsilon = RT \ln\left(1 + \frac{1}{C_e}\right) \tag{8}$$

$$E = (2k_{ad})^{-0.5} \tag{9}$$

where R is the universal gas constant (8.314 J mol^{-1} K^{-1}) and T is temperature (°K). A dimensionless constant (R_L) representing the affinity of an adsorbent and adsorbate system was calculated based on the K_L of the Langmuir isotherm using Eq. (10);

$$R_L = \frac{1}{1 + K_L C_0} \tag{10}$$

where, C_0 is the initial adsorbate concentration.

2.4. Evaluation of CIP adsorption at different pHs

The adsorption capacity of CIP to AB and AS was measured at a pH range of 2.2–10.5. The pH was adjusted using 0.1 M HCl and 0.1 M NaOH. The initial CIP concentrations were 100 and 33 mg L^{-1} for AB and AS, respectively. The adsorbent doses were 0.04 and 0.22 g dry weight for AB and AS, respectively. 50 ml vials were used and shaken at 150 rpm for 24 h at RT during these adsorption experiments.

2.5. CIP biodegradation test

Removal routes of CIP in the bioreactors at steady state were determined using glass separate flasks where the same bioreactor operational conditions were established. The mixed liquor suspension including AB was taken from AB40 at day 42. Biofilms attached on AB were detached using vortexing (30 s), followed by sonication (1 min) as described previously [25]. Both the suspended and detached biofilm biomasses were mixed, washed using PBS, and resuspended into glass flasks with 1 mg L^{-1} CIP-containing synthetic feed. The glass flasks were maintained with operational conditions identical to the bioreactors and CIP concentrations were followed for 96 h.

2.6. Characterizing surface properties of AB and AS

Surfaces (e.g., microstructure and attached biofilm) of AB were visualized using a scanning electron microscopy (SEM). AB specimens were taken from AB40 at day 42. Biofilms on AB surfaces were fixed using 2.5 % glutaraldehyde in PBS for 2 h. The fixed specimens were dehydrated with ethanol following the procedures previously described [26]. The ethanol-treated specimens were dried at 105 °C for 12 h and sputtered with platinum (Pt) to a thickness of 5 nm. The pre-treated AB specimens were subjected to the MERLIN field emission scanning electron microscope (FE-SEM; Carl Zeiss, Germany). Fourier-transform infrared (FTIR) spectra were obtained using powders of AB and AS ground to less than 50 μm in diameter. The ground samples were dried in a freeze dryer (FDB 5503, Operon, Korea) for 3 days. The potassium bromide (KBr) pellets were prepared containing 0.25 % of AB or AS and KBr. IR-spectra were determined using a Nicolet iS10 FTIR spectrophotometer (Thermo Scientific, USA) in the wavenumber range of 4,000–400 cm^{-1}. The zeta potential was measured at a concentration of 5 g samples in 1 L 0.01 M KCl aqueous solution, using a zeta potential analyzer (ZetaPlus, Malvern, UK), at a pH range of 3–10. Specific surface area was analyzed using nitrogen physisorption with Brunauer–Emmelt–Teller (BET) method (BELSORP-max; BEL, Japan).

2.7. Analytical methods

CIP (CAS number: 85721-33-1) was purchased from Sigma-Aldrich Korea. A CIP stock solution (100 mg L^{-1}) was prepared in DIW and stored in amber bottles at 4 °C until use. The concentration of CIP was determined using a YL9100 high-performance liquid chromatography system (Young-Lin Instrument Co. Ltd., South Korea) with an ultraviolet detector (278 nm) [19]. Chromatographic separation was conducted at 30 °C on a Zorbax Eclipse Plus C18 column (250 mm × 4.6 mm id, 5 μm; Agilent, USA) at 1.0 mL min^{-1} of a flow rate with 100 μL of the injection volume. The mobile phase was prepared in 25 mM NaH_2PO_4 adjusted to pH 2.5 using phosphoric acid and mixed with acetonitrile (82:18 v/v). COD, NH_4^+-N, and VSS were measured according to standard methods [27]. The Mann-Whitney U test was performed to assess statistical significance on differential characteristics.

3. Results and discussion

3.1. Performance of AB-dosed AS on antibiotic control

Fig. 1A shows the concentration of CIP in each reactor effluent for the entire period of reactor operation from reactor start-up to quasi-steady state. All effluent CIP concentrations were less than 0.2 mg L^{-1} at day 3.5 (the end of the first feeding cycle), after which CIP removal performance differed significantly among the reactors. The control reactor rapidly increased the CIP effluent concentration and showed non-detectable removals at days 24–42. While the CIP levels of the AB10 and AB20 effluents gradually increased and leveled off at days 24–42, AB40 could limit the effluent CIP level below 0.025 mg L^{-1} throughout the entire cycles (Fig. 1A). The average CIP removal rate during steady state (24–42 days) was 35.5 ± 0.5 %, 54.1 ± 0.7 % and 94.3 ± 0.7 % for AB10, AB20 and AB40, respectively, whereas the control system showed negligible removals (< 0.5 %). Although a single reactor was run with each condition, the CIP removal performance was quite stable at steady state, suggesting little stochastic variation in the reactor performance. The CIP removal rate of AB10, AB20, and AB40, respectively, at steady state was significantly higher than ($P < 0.05$ by Mann-Whitney U test) that of the control reactor. The OLS regression analysis (Fig. S1) of the CIP removal rates at steady state in relation to the AB volumetric ratio further revealed a significantly positive relationship ($r = 0.99$ with $P < 0.05$), strongly suggesting the critical role of AB on controlling the fate of CIP.

CIP removal in a laboratory-scale membrane bioreactor with 15 g L^{-1} mixed liquor suspended solids was 53 % [28] and an up-flow biological aerated filter reached approximately 78 % [29], while the removal rate of an anaerobic reactor was found to be relatively low (15–40 %) [30]. A sulfate-reducing up-flow sludge bed reactor displayed 90 % removal from 1 mg L^{-1} CIP-containing influent, which decreased to 65 % with an increase of CIP influent concentration to 5 mg L^{-1} [31]. Considering the removal rates previously reported, direct dosage of AB to AS, with its 40 % AB filling ratio, was found to provide outstanding performance on CIP removal relative to other biological systems as well as the control (i.e., AS alone) used in this study.

The potential effects of AB dosage on the essential performances (organic matter and ammonia nitrogen removals) of AS were examined. Fig. 1B shows soluble organic matter (represented by soluble COD [sCOD]) removal in the effluents from the control and three AB-dosed reactors. While the bioreactors were fed by the influent with 2,000 mg L^{-1} of sCOD for the entire feeding cycles, effluent sCOD concentrations were 198 ± 12 mg L^{-1} in the first feeding cycle and remained stable (45–65 mg L^{-1}) at days 14–42. All reactors achieved high levels of steady state sCOD removal rates (> 97 %). In addition, all reactors showed similar VSS levels (1.0–1.3 g L^{-1}) and NH_4^+-N removal rates (46–50 %) at steady state. These results collectively suggested that organic matter, ammonia removal, and biomass yield of AS dosed with 10–40 % AB volumetric ratios addition were comparable to those of the control reactor, suggesting that direct addition of AB into activated sludge may not affect/disrupt the key original performances (i.e., removals of conventional organic contaminants) while significantly improving controlling antibiotic waste streams.

3.2. Role of AB as a microbial carrier on antibiotic removal

The surfaces of the virgin (as-purchased), nitric acid-treated, and biofilm-attached AB are visualized in Fig. 2. The biofilm-attached AB was sampled from AB40 at steady state. Compared with Fig. 2A (virgin), Fig. 2B shows holes and macropores with less impurities, suggesting that nitric acid pre-treatment effectively eliminated debris and impurities. Fig. 2C clearly illustrates a non-homogenous, irregularly aggregated biofilm distribution on the surface, including cocci-like bacteria. A feedstock material used for pyrolysis affects the microstructure of the biochar surface and its physicochemical properties

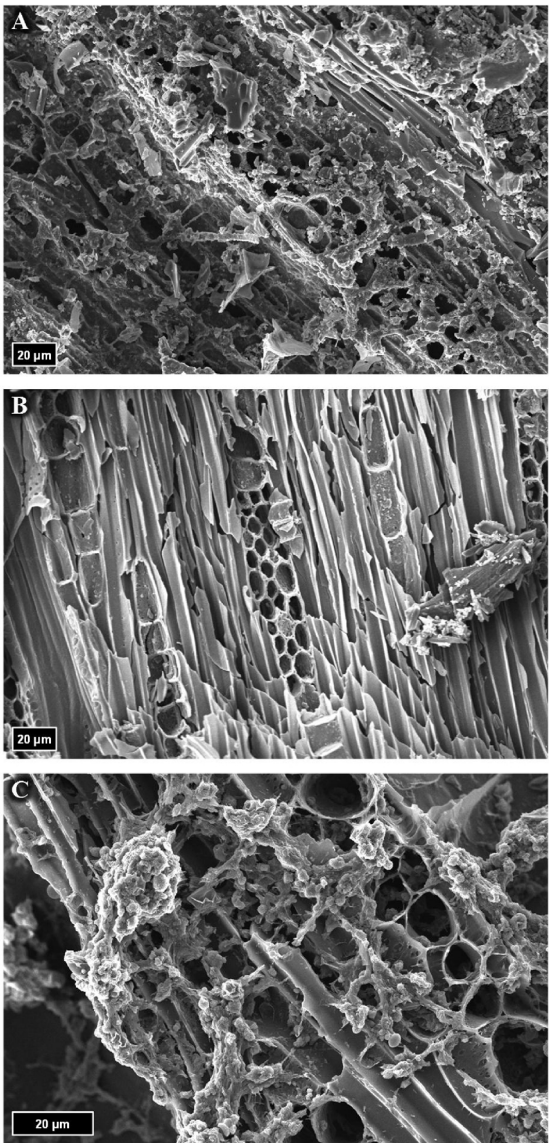

Fig. 2. SEM images of virgin (A), nitric acid-treated (pretreated) (B), and biofilm-attached (C) biochar. The dark boxes supply scales.

[32]. The surface structure of AB resembled that of biochar derived from a typical hardwood, with fiber cells, vessels, and large pore spaces, as observed by Gibson [33]. Cocci-like bacteria observed in the AB (Fig. 2C) are often found in AS flocs and designated “G-bacteria” by morphology, which include phylogenetically diverse organisms that play a role in aerobic degradation of organic matter in AS [34].

The biofilm attached to AB visualized in Fig. 2C and the outstanding CIP removal that occurred in AB40 (Fig. 1) both at steady state led us to examine the potential contribution of biomass on the CIP removal. Both suspended and biofilm biomasses were taken from AB40 and inoculated into separate glass flasks (with other experimental conditions identical to those of AB40) fed with 1 mg L^{-1} of CIP. The abiotic condition was established without biomass inoculation and the biotic condition with both suspended and biofilm biomasses. Time-course CIP concentrations in the two conditions were followed over four days (Fig. S1), slightly longer than a feeding cycle duration. The CIP levels did not change (< 0.01 mg L^{-1} of change) in the abiotic condition, whereas slightly decreasing CIP (0.98 mg L^{-1} and 0.94 mg L^{-1} at day 1 and 4, respectively) was detectable in the biotic condition, suggesting a minor contribution of biosorption/biodegradation to the overall CIP removal. Since the tempo of the biotic removal was comparable to the previous

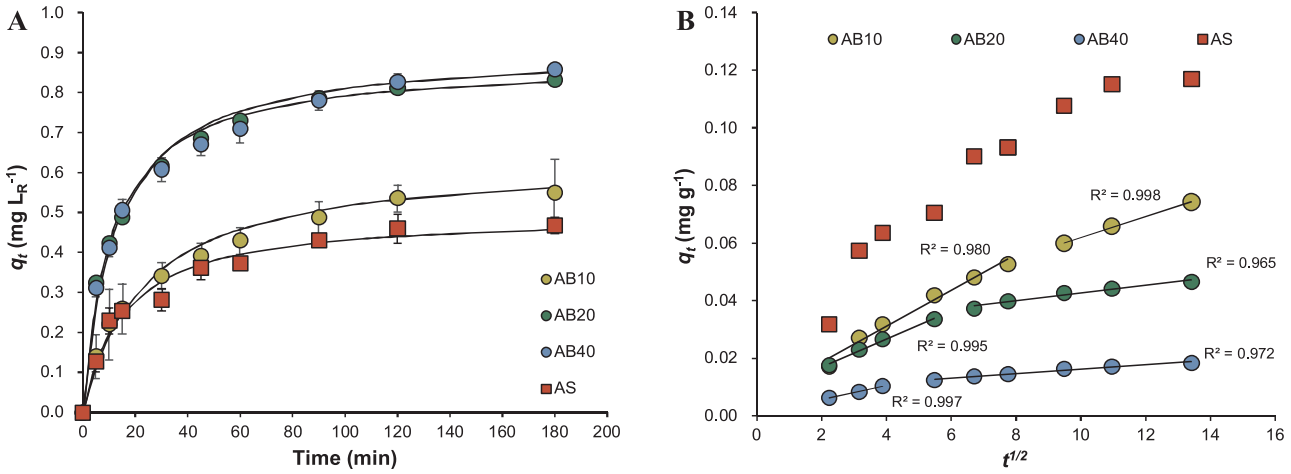

Fig. 3. Kinetics of CIP adsorption to AB with different filling ratio and AS. (A) Time course of CIP adsorption amount. The line represents the pseudo-second-order adsorption kinetic model prediction. The symbols and error bars represent the mean (n = 3) and the standard deviation, respectively. (B) CIP adsorption characterized by the Weber–Morris intraparticle diffusion model. Each symbol represents the mean of triplicate measurements with < 5 % of standard deviation from the mean.

kinetics estimate (about 0.01–0.08 d^{-1}) [10], our and previous study collectively suggested that CIP in the biotic conditions is relatively stable and persistent.

3.3. Adsorption kinetics of CIP on AB and AS

Micropollutants such as pharmaceutical and personal care products and industrial chemicals in CASP are removed with various routes through biodegradation, sorption, hydrolysis/photolysis, and volatilization [22]. AB indeed acted as a microbial carrier (Fig. 2C). Since the biological removal extent observed in a separate flask was much less significant than the overall CIP removals (94 %) that occurred in the AB-dosed bioreactors at steady state, which prompted further investigation on the contribution of other removal routes (e.g., CIP adsorption to AB). Pretreated AB (using nitric acid) and AS directly taken from an aeration tank of a full-scale WWTP, neither of which had been exposed to CIP, were used for characterizing adsorption kinetics. Fig. 3A shows time-course adsorption of CIP in glass vials with 10 %, 20 %, and 40 % of AB and 3 g VSS L^{-1} of AS, respectively, simulating the same settings established in the three AB-dosed and control reactor. In contrast to the minor CIP removal contributed by biomass over the four days (Fig. S1), CIP was rapidly and substantially removed within three hours (Fig. 3A). The pseudo-second-order kinetic model was the best fit (r^2 > 0.99) for the experimental results with the hardwood-based biochar, as previously reported for adsorption of a range of trace organic pollutants, including CIP, to other types of biochars [17–19,35]. The adsorption rate constant per unit volume (L_R) varied with AB volumetric ratios similarly simulated as in the AB-dosed reactors was assessed: AB40 (48.1 L_R mg^{-1} min^{-1}) > AB20 (7.4) > AB10 (1.1) > AS (0.4). The q_e value was in the order of AB40 (0.776 mg L_R^{-1}) > AB20 (0.772) > AB10 (0.513) > AS (0.432). The much faster and greater adsorption to AB than AS highlighted the significant contribution of the AB-mediated CIP adsorption removal rather than the AS-mediated biosorption in the AB-dosed reactors at steady state.

While adsorption to AB and AS could be described well with the pseudo-second-order kinetic model, only AB-mediated adsorption (not AS-mediated) was fitted well to the Weber–Morris intraparticle diffusion model (multilinear plots with r^2 > 0.96 in Fig. 3B), suggesting intraparticle diffusion could be more significant in AB-mediated adsorption relative to AS. Adsorption processes consist of three steps: 1) boundary-layer diffusion within the layer on the adsorbent surface, 2) intra-particle diffusion of adsorbates into the pores and 3) adsorption on the adsorption sites either on the surface or in the pores of adsorbents, which is fast and not rate-limiting [36]. The kinetics results suggested that CIP was adsorbed onto the adsorption sites on the outer surface of AB, which is easily accessible, in the first linear stage, while CIP was transported into the sites in inner pores with higher resistance in the second linear stage. We also observed that the period of the first stage increased as the amount of AB increased, providing more outer surfaces. The intercept of the plots, i.e., c in Eq. (3), was significantly smaller than q_e, indicating that the boundary layer played a minor role in adsorption.

3.4. Adsorption isotherm of CIP on AB and AS

Fig. 4 illustrates the increasing adsorption capacity of CIP with the increase of CIP liquid concentration. The maximum adsorption capacity obtained using the Langmuir isotherm (a better fit to the experimental results than other models) was 20.7 and 5.0 mg g^{-1} (Table 2), while R_L was in a range of 0.30–0.81 and 0.28–0.94 for AB and AS, respectively. Given the adsorption behaviors classified based on R_L values: irreversible (0), favorable (0–1), and unfavorable (> 1) [24], CIP adsorption to both AB and AS was found to be favorable. The maximum CIP adsorption capacity values measured in this study were in an agreement with previous estimates: 10–96.3 mg g^{-1} by various types of biochar (Table S1) and 3.4 by AS [37]. These results supported the greater CIP adsorption capacity by the AB-dosed reactors for the longer period (Fig. 1A).

The good fit of the Langmuir isotherm model and the unity (1.00) of β (Sips isotherm) suggested that CIP adsorption onto both BC and AS could be accomplished through monolayer and homogeneous adsorption and that adsorption enthalpy was not affected by surface coverage [24]. Experimental data were fitted to the Dubinin–Kaganer–Radushkevich isotherm model to infer apparent adsorption energy, since it is often used to describe the adsorption mechanism with a Gaussian energy distribution onto a heterogeneous surface [24]. The adsorption mechanism can be predicted depending on the apparent free energy of adsorption (E): physical (E < 8), ion exchange (8 < E < 16), and strongly chemical (E > 16) [24]. The E value was 9.4 and 11.8 kJ mol^{-1} for AB and AS, respectively, implying that adsorption occurred primarily by ionic exchange between ionizable protons on the acidic surface [–Cπ–H_3O^+]) [38] and/or the exchange of electrons between adsorbates and adsorbents [39].

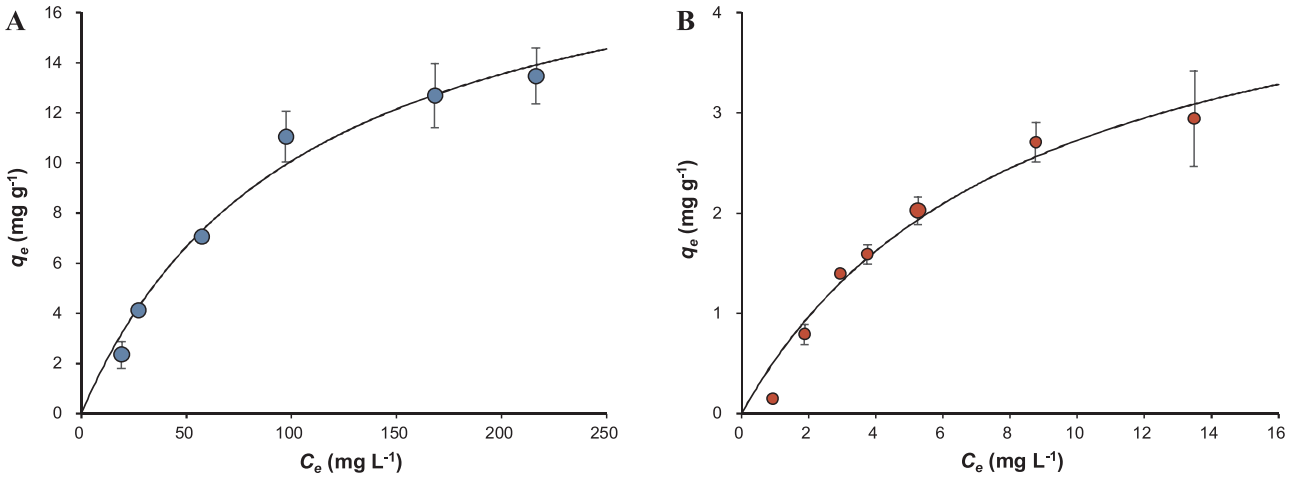

Fig. 4. Modeling of CIP adsorption isotherm with (A) AB and (B) AS. Solid lines represent the Langmuir isotherm model prediction. The symbols and error bars represent the mean (n = 3) and standard deviation, respectively.

3.5. CIP-mediated shifts in surface properties

Fig. 5A presents the FTIR spectra of the pre-treated and CIP-adsorbed AB, which identified the presence of the O—H bond in hydroxyl functional groups (the band observed at 3200–3500 cm^{-1}), aliphatic CH_2 asymmetric stretch (2917 cm^{-1}), aliphatic CH_2 symmetric stretch (2850 cm^{-1}), the stretching of symmetric and asymmetric vibration of C═O in CO_2 (2360 cm^{-1}), ketonic and carboxylic C═O (1703 cm^{-1}), C═C of the aromatic ring or highly conjugated C═C bond generated during pyrolysis of raw material (1595 cm^{-1}), and bending vibration of methyl (1384 cm^{-1}). The presence of CO_2 (2360 cm^{-1}) was probably attributed to the low temperature during manufacture of the AB, often detected in those of other types of biochars under slow pyrolysis at relatively low temperatures (400 °C) [40]. The peak at 1270 cm^{-1} assigned to a phenolic C—OH bond was probably attributable to adsorbed CIP molecules. In addition, the peak of aromatic C═C bonds shifted from 1595 to 1583 cm^{-1}, indicating that π-π electron-donor-acceptor (EDA) interactions contributed to the adsorption [41]. The carbon atom bonded to fluorine (C═C*-F) in CIP molecules is a π-electron-acceptor due to the strong electron-withdrawing ability of fluorine [42]. The π-π EDA interactions in the organic compounds adsorption by carbon-based materials contribute significantly to the adsorption of aromatics to biochar and graphitic materials [19,43].

The spectrum (Fig. 5B) of AS and CIP-adsorbed AS included peaks associated with the O—H of a hydroxyl group compound (polyalcohol and saccharides, 3200 ~ 3500 cm^{-1}), the vibration H-bonds between OH groups of cellulose and NH in the amide groups (3280 cm^{-1}), the stretching vibration of C—H stretch (2924 cm^{-1}), C-H_2 asymmetric and symmetric stretch (2852 cm^{-1}), stretching asymmetrical vibrations of COO^- in peptides and proteins (1652 cm^{-1}), stretching vibration of C—N and N—H of amide II of the protein polymer (1548 cm^{-1}), NH_3^+ in peptide (1402 cm^{-1}), and C—O—C of amide III or aromatic ethers (1242 cm^{-1}) [44]. The intensities of all peaks at 3280–1652 cm^{-1} decreased after CIP adsorption, indicating that a variety of functional groups on AS surfaces were involved in CIP adsorption. Zhang et al. [45] found that most of the functional groups of extracellular polymeric substances of aerobic sludge, including carboxyl, hydroxyl, and amine bind with CIP. They also reported that EPS contributed to approximately 50 % of CIP removal by aerobic sludge. Meanwhile, a peak at 1032 cm^{-1} appearing after CIP adsorption represented the C—F stretching of CIP, supporting the CIP adsorption onto AS.

3.6. Effects of pH on Zeta potential and CIP adsorption

Fig. 6A shows the zeta potential and the CIP adsorption amount of AB under different pHs. The zeta potential of AB was −21.7 mV at pH 3.1, decreased to −49.3 mV at pH 6, and then further decreased 51.7 mV at pH 10.0. Biochars show a range of zeta potential from −20 to 0 mV at pH 3.5, which decreases as pH increases [46]. The point of zero charge is 3.05 for a tea-leaf biochar [19]. The surface charge of AB was significantly more negative than those previously reported, suggesting that the AB used in this study could have a high adsorption potential to

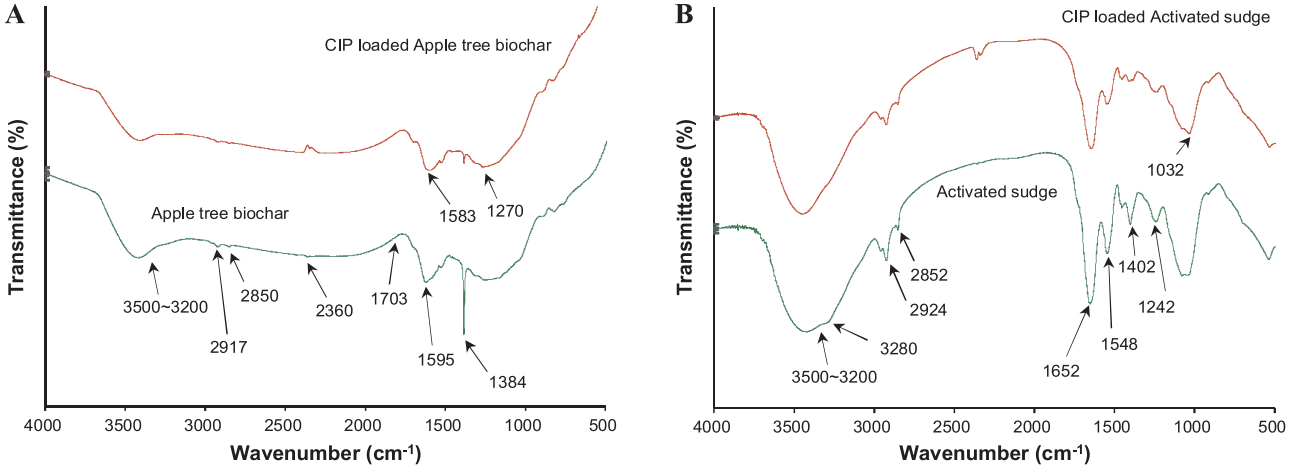

Fig. 5. (A) FTIR spectra of AB and CIP-adsorbed AB. (B) FTIR spectra of AS and CIP-adsorbed AS.

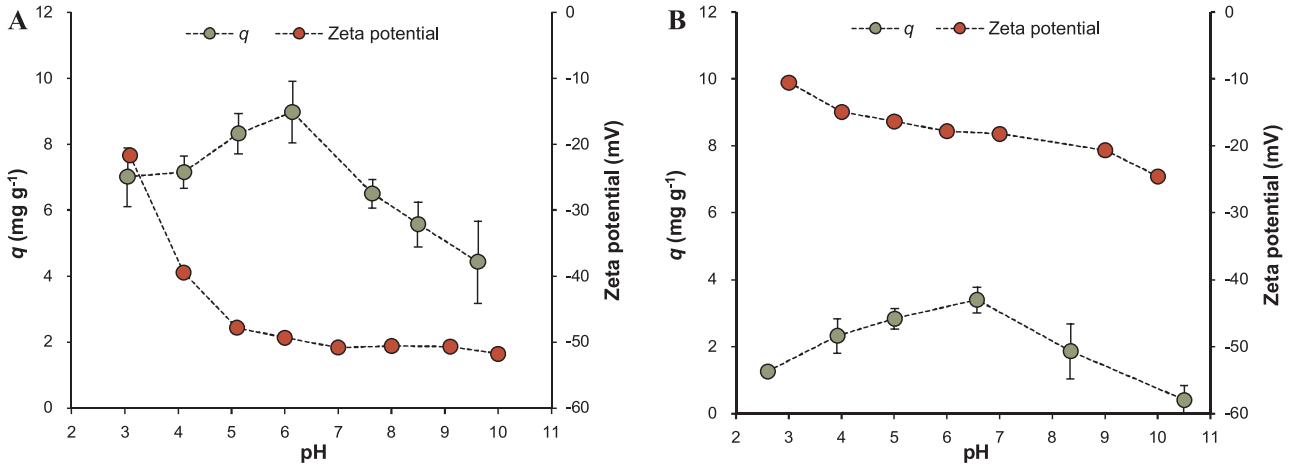

Fig. 6. Zeta potential and CIP adsorption potential at a range of pH. (A) CIP adsorption to AB. (B) CIP adsorption to AS. The symbols and error bars represent the mean (n = 3) and standard deviation, respectively.

cationic metals via higher electrostatic attraction.

The highest CIP adsorption potential was recorded at pH 6.3 and decreased whether the pH rose or fell. The optimum CIP adsorption of AB was at the pH range relevant to those in municipal wastewaters, consistent with other studies [19,35]. The highest adsorption achieved at a nearly neutral pH was attributable to strong hydrophobic effects and π-π EDA interactions. CIP exists dominantly as a cation ($CIPH_2^+$), zwitterion ($CIPH^\pm$) and anion (CIP^-) when the pH is < 5.9, 6.1–8.7 and > 8.9, respectively, because of the two dissociation constants (pKa) of CIP. One of the pKas is 5.9 for the carboxylic acid group and the other is 8.8 for the amine group on the piperazine moiety. $CIPH^\pm$ has the highest hydrophobicity among three CIP species [43] and is an effective π-electron-acceptor, taking part in strong π-π EDA interactions with the graphite structures of the AB. The pH-dependent adsorption observed in Fig. 6A could be attributable to several mechanisms. As pH decreases, the π-electron accepting ability of CIP increases (i.e., favorable to adsorption), while the electrostatic attraction and hydrophobicity decrease (i.e., unfavorable to the adsorption) [47]. Therefore, hydrophobicity and the electrostatic repulsion likely dominantly affected CIP adsorption under acidic pH. In contrast, as pH increases, the electrostatic attraction, the π-electron accepting ability, and hydrophobicity decrease due to deprotonation and ionization [48], which are all unfavorable to the adsorption, which led to a significant decrease of CIP adsorption.

The zeta potential and the CIP adsorption of AS at a range of pH values are presented in Fig. 6B. The surface of AS is negative due to the ionization of the anionic functional groups, such as carboxylic acid and phosphate [49]. The zeta potential of AS taken from oxic tanks of three municipal WWTPs was in a range of −0.1 to −5 at pH 3 and of −20 to −30 at pH 12 [50]. The zeta potential of AS was 0 to −5 mV at pH 3 and decreased to −20 mV at pH 7 [51].

The CIP adsorption potential onto AS was the highest at pH 6.3 and fell as pH either increased or decreased, as observed with AB. The adsorption of $CIPH^\pm$ at nearly neutral conditions could be due to a combination of electrostatic attraction, cation exchange of the protonated amine, cation bridging of divalent cations, and the anionic carboxyl group of $CIP^\pm$ [52]. These results suggested that CIP adsorption to AS may be suppressed by protonation of anionic carboxyl groups under acidic conditions and/or by the increase of electrostatic repulsion under alkaline condition.

3.7. CIP removals in AB-dosed AS systems: mechanism and practical implication

While several studies have documented CIP adsorption to biochars with other biomass sources [19,35], little is known about the characteristics and mechanism of CIP adsorption to hardwood-based biochar. This work provided insights into mechanisms facilitating CIP adsorption to AB, a hardwood-derived biochar. First, the CIP adsorption kinetics could be primarily governed by the diffusion within macropores rather than meso/micropores. It was supported by the kinetics model (Webber-Morris) (Fig. 3A and Table 1) and significantly larger macropores relative to mesopores and micropores. The latter was experimentally validated with the SEM images (Fig. 2B) and the smaller volume (0.00887 and 0.00265 $cm^3\ g^{-1}$) and specific surface area (2.02 and 2.33 $m^2\ g^{-1}$) of mesopores and micropores, respectively, measured using the BET analysis. Second, the CIP adsorption to AB also involved hydrophobic effects of CIP, π- π EDA interactions, and electrostatic attraction between CIP and AB, inferred from the surface characterization results (Figs. 5 and 6). The proposed mechanism was also supported by the apparent adsorption energy (E of the Dubinin–Kaganer–Radushkevich isotherm, Fig. 4 and Table 2).

Direct dosage of AB into AS could greatly enhance CIP removal (Fig. 1A) largely via adsorption to AB rather than biodegradation/biosorption. Because the biomass tested in this study was taken from

Table 1
Parameters of adsorption kinetic models.

Model		Parameter	AB10	AB20	AB40	AS
Pseudo-		k_{a1} (min^{-1})	0.041	0.072	0.069	0.052
first-		q_e ($mg\ g^{-1}$)	0.063	0.042	0.016	0.108
order		q_e ($mg\ L_R^{-1}$)	0.513	0.772	0.776	0.432
		r^2	0.962	0.963	0.954	0.941
Pseudo-		k_{a2} ($g\ mg^{-1}\ min^{-1}$)	0.680	2.00	4.91	0.522
second-		k_{a2} ($L_R\ mg^{-1}\ min^{-1}$)	1.11	7.35	48.1	0.418
order		q_e ($mg\ g^{-1}$)	0.073	0.047	0.018	0.124
		q_e ($mg\ L_R^{-1}$)	0.599	0.867	0.878	0.496
		r^2	0.991	0.994	0.991	0.998
Intra-	First	k_{diff} ($g\ mg^{-1}\ min^{-1/2}$)	6.23 × 10^{-3}	4.87 × 10^{-3}	2.42 × 10^{-3}	–
particle	stage	c ($mg\ g^{-1}$)	6.21 × 10^{-3}	7.30 × 10^{-3}	0.90 × 10^{-3}	–
diffusion		r^2	0.980	0.995	0.997	–
	Second	k_{diff} ($g\ mg^{-1}\ min^{-1/2}$)	3.64 × 10^{-3}	1.36 × 10^{-3}	0.77 × 10^{-3}	–
	stage	c ($mg\ g^{-1}$)	2.55 × 10^{-2}	2.91 × 10^{-2}	0.86 × 10^{-2}	–
		r^2	0.998	0.965	0.972	–

Note. The mean value of triplicate measurements at each time point was used for model prediction.

Table 2
Parameters of adsorption isotherms.

Model	Parameter	AB	AS
Langmuir	$q_{max,L}$ (mg g^{-1})	20.7	4.99
	K_L (L mg^{-1})	0.0095	0.1205
	r^2	0.98	0.97
Freundlich	K_F	0.713	0.654
	$1/n$	0.559	0.613
	r^2	0.94	0.92
Sips	$q_{max,S}$ (mg g^{-1})	20.7	4.99
	K_S (L mg^{-1})	0.0095	0.1205
	β	1.00	1.00
	r^2	0.98	0.97
Dubinin–Kaganer–Radushkevich	q_S (mg g^{-1})	31.8	11.7
	E (kJ mol^{-1})	9.38	11.8
	r^2	0.96	0.98

Note. The mean value of triplicate measurements at each time point was used for model prediction.

the AB-dosed reactor at steady state, CIP likely had been already adsorbed to the biomass, therefore severely limiting further biosorption-mediated CIP removal that could possibly occur. In contrast, the AS samples freshly taken from full-scale WWTPs showed rapid and significant biosorption potential, highlighting considerable sorption potential to AS (Figs. 3 and 4 and Tables 1 and 2). Accordingly, CIP removals observed in the control reactor until day 21 could occur via biosorption to suspended biomass. Compared with the limited adsorption capacity by suspended biomass in the control system at steady state, addition of AB could significantly improve the removal capacity (94 % CIP removals in AB40). Our adsorption kinetics and isotherm parameters demonstrated the high adsorption rate, maximum adsorption capacity, and affinity of CIP to AB (Figs. 3 and 4 and Tables 1 and 2). The CIP concentration tested in this study greatly exceeds the typical levels of CIP (e.g., less than dozens of μg L^{-1}) in municipal wastewater influents, suggesting that AB-dosage might be effective for treating CIP-bearing waste streams at a wide range of environmentally relevant levels. Despite the effectiveness, given that municipal waste streams carry a lot of organic and inorganic compounds that may compete/interfere with the antibiotic adsorption to biochar, we should therefore suggest further experimental investigations (e.g., antibiotic removal performance, breakthrough time, and regeneration strategy of biochar) of the removal performance, using both the bench and pilot-scale AS systems dosed with biochar receiving real wastewaters.

CIP removals in full-scale WWTPs are often attributed to biosorption onto AS biomass [12,52], while CIP represents a poorly biodegradable micropollutant [52]. The disappearance of CIP resulting from adsorption to wasted AS (WAS), not biodegradation, may give rise to another critical issue, as the CIP released with WAS may perturb ecosystems of post-treatment processes (e.g., anaerobic digestion) and biosolid-amended sites. For example, our previous study revealed that > 0.5 mg L^{-1} of CIP could cause significant inhibition on aerobic activated sludge (e.g., potential heterotrophic and nutrient removal activities) and anaerobic methanogenic sludge (e.g., fermentation and methane production activities) with alteration on the microbial community structure and diversity [7]. Given the faster and higher adsorption capacity of AB than AS, dosing biochar into AS would help effectively remove CIP from the WAS as well as the wastewater effluents.

The performances of biochar-dosed bioreactors can be further improved through modifying surface properties of biochar. There are many factors (e.g., biomass feedstock, pyrolysis condition such as temperature, and pretreatment) affecting the surface properties (e.g., surface-to-volume ratio) of biochar and thus potentially enhancing the treatment performance (adsorption kinetics/isotherm). Hence, the AB dosage (10–40 %) tested in this study (Fig. 1) may be further reduced through surface modification of biochar as both an adsorbent and a microbial carrier. Despite its great adsorption capacity of biochar as observed in this study (Figs. 3 and 4), biochar has a finite adsorption capacity. Once biochar reaches its maximum adsorption capacity, the used biochar, as activated carbon materials, would be disposed to landfills/incinerators or regenerated (recycled). A variety of regeneration methods for biochar using thermal energy, solvent, microwave, and supercritical fluid have been developed [53], which may significantly extend the life of biochar and thus reduce the operational cost. The technical feasibility of biochar addition into AS for micropollutant removal observed in this study strongly suggests future investigations on the surface modification and regeneration methods of biochar.

4. Conclusions

AS reactors with varied AB volume ratios were established for treating antibiotic wastewaters. Removal efficiency of CIP was correlated with the added amount of AB, achieving up to 94 % of CIP removals by AB-dosed AS reactors, while a control AS reactor without AB showed a non-detectable removal. Adsorption kinetics and isotherm results suggested the majority of CIP was removed by adsorption onto AB primarily via intraparticle diffusion, π-π EDA interaction, and hydrophobic and electrostatic attraction. The outstanding CIP removal rates observed in this work proposed that direct dosage of biochar into AS system may be a cost-effective and simple alternative treatment option for antibiotic-bearing waste streams.

Declaration of Competing Interest

The authors declare that they have no known competing financial interests or personal relationships that could have appeared to influence the work reported in this paper.

Acknowledgments

This work was supported by a Korea Environment Industry & Technology Institute (KEITI) through Subsurface Environmental Management (SEM) Projects, funded by Korea Ministry of Environment (MOE) (2019002480005).

Appendix A. Supplementary data

Supplementary material related to this article can be found, in the online version, at doi:https://doi.org/10.1016/j.jwpe.2019.101019.

References

[1] R.K. Nam, R. Saskin, Y. Lee, Y. Liu, C. Law, L.H. Klotz, Increasing hospital admission rates for urological complications after transrectal ultrasound guided prostate biopsy, J. Urol. 189 (2013) S12–S17.
[2] W. Castro, M. Navarro, C. Biot, Medicinal potential of ciprofloxacin and its derivatives, Future Med. Chem. 5 (2013) 81–96.
[3] S. Sahlin, D.G.J. Larsson, M. Ågerstrand, Ciprofloxacin: EQS data overview, The Department of Environmental Science and Analytical Chemistry (ACES) Report 15, Stockholm University, Stockholm, 2018.
[4] A. Hartmann, E.M. Golet, S. Gartiser, A.C. Alder, T. Koller, R.M. Widmer, Primary DNA damage but not mutagenicity correlates with Ciprofloxacin concentrations in German hospital wastewaters, Arch. Environ. Contam. Toxicol. 36 (1999) 115–119.
[5] A.A. Robinson, J.B. Belden, M.J. Lydy, Toxicity of fluoroquinolone antibiotics to aquatic organisms, Environ. Toxicol. Chem. 24 (2005) 423–430.
[6] Y. Luo, W. Guo, H.H. Ngo, L.D. Nghiem, F.I. Hai, J. Zhang, S. Liang, X.C. Wang, A review on the occurrence of micropollutants in the aquatic environment and their fate and removal during wastewater treatment, Sci. Total Environ. 473–474 (2014) 619–641.
[7] D. Kim, L.N. Nguyen, S. Oh, Ecological impact of the antibiotic ciprofloxacin on microbial community of aerobic activated sludge, Environ. Geochem. Health (2019), https://doi.org/10.1007/s10653-019-00392-6.
[8] P. Verlicchi, M. Al Aukidy, E. Zambello, Occurrence of pharmaceutical compounds in urban wastewater: removal, mass load and environmental risk after a secondary treatment-a review, Sci. Total Environ. 429 (2012) 123–155.
[9] I.A. Parshikov, T.M. Heinze, J.D. Moody, J.P. Freeman, A.J. Williams, J.B. Sutherland, The fungus Pestalotiopsis guepini as a model for biotransformation

of ciprofloxacin and norfloxacin, Appl. Microbiol. Biotechnol. 56 (2011) 474–477.
[10] J.Q. Xiong, M.B. Kurade, J.R. Kim, H.S. Roh, B.H. Jeon, Ciprofloxacin toxicity and its co-metabolic removal by a freshwater microalga Chlamydomonas mexicana, J. Hazard. Mater. 323 (2017) 212–219.
[11] L.N. Nguyen, L.D. Nghiem, S. Oh, Aerobic biotransformation of the antibiotic ciprofloxacin by Bradyrhizobium sp. isolated from activated sludge, Chemosphere 211 (2018) 600–607.
[12] A. Jia, Y. Wan, Y. Xiao, J. Hu, Occurrence and fate of quinolone and fluoroquinolone antibiotics in a municipal sewage treatment plant, Water Res. 46 (2012) 387–394.
[13] K.A. Thompson, K.K. Shimabuku, J.P. Kearns, D.R.U. Knappe, R.S. Summers, S.M. Cook, Environmental comparison of biochar and activated carbon for tertiary wastewater treatment, Environ. Sci. Technol. 50 (20) (2016) 11253–11262.
[14] L. Sbardella, J. Comas, A. Fenu, I. Rodriguez-Roda, M. Weemaes, Advanced biological activated carbon filter for removing pharmaceutically active compounds from treated wastewater, Sci. Total Environ. 636 (2018) 519–529.
[15] J. Streicher, A.S. Ruhl, R. Gnirß, M. Jekel, Where to dose powdered activated carbon in a wastewater treatment plant for organic micro-pollutant removal, Chemosphere 156 (2016) 88–94.
[16] F.R. Oliveira, A.K. Patel, D.P. Jaisi, S. Adhikari, H. Lu, S.K. Khanal, Environmental application of biochar: current status and perspectives, Bioresour. Technol. 246 (2017) 110–122.
[17] C. Chen, W. Zhou, D. Lin, Sorption characteristics of N-nitrosodimethylamine onto biochar from aqueous solution, Bioresour. Technol. 179 (2015) 359–366.
[18] T. Chen, L. Luo, S. Deng, G. Shi, S. Zhang, Y. Zhang, O. Deng, L. Wang, J. Zhang, L. Wei, Sorption of tetracycline on H3PO4 modified biochar derived from rice straw and swine manure, Bioresour. Technol. 267 (2018) 431–437.
[19] J. Li, G. Yu, L. Pan, C. Li, F. You, S. Xie, Y. Wang, J. Ma, X. Shang, Study of ciprofloxacin removal by biochar obtained from used tea leaves, J. Environ. Sci. 73 (2018) 20–30.
[20] J.C. Leyva-Díaz, J. Martín-Pascual, J.M. Poyatos, Moving bed biofilm reactor to treat wastewater, Int. J. Environ. Sci. Technol. 14 (2017) 881–910.
[21] N.A. ElNaker, M. Elektorowicz, V. Naddeo, S.W. Hasan, A.F. Yousef, Assessment of microbial community structure and function in serially passaged wastewater electro-bioreactor sludge: an approach to enhance sludge settleability, Sci. Rep. U. K. 8 (2018) 7013.
[22] S. Oh, S. Choi, Microbial community enhances biodegradation of bisphenol A through selection of Sphingomonadaceae, Microbial Ecol. 77 (2018) 631–639 2019.
[23] W.J. Weber, C. Morris, Kinetics of adsorption on carbon from solution, J. Sanity. Eng. Div. Am. Soc. Civil Eng. 89 (1963) 31–59.
[24] K.Y. Foo, B.H. Hameed, Insights into the modeling of adsorption isotherm systems, Chem. Eng. J. 156 (2010) 2–10.
[25] N. Kobayashi, T.W. Bauer, M.J. Tuohy, T. Fujishiro, G.W. Procop, Brief ultrasonication improves detection of biofilm-formative bacteria around a metal implant, Clin. Orthop. Relat. Res. 457 (2007) 210–213.
[26] K. Leinweber, P.G. Kroth, Capsules of the diatom Achnanthidium minutissimum arise from fibrillar precursors and foster attachment of bacteria, Peer J. 3 (2015) e858, https://doi.org/10.7717/peerj.858 2015.
[27] APHA, AWWA, WEF, Standard Methods for the Examination of Water and Wastewater, 22nd ed., (2012) Washington, DC.
[28] N. Dorival-García, A. Zafra-Gómez, A. Navalón, J. González, J.L. Vílchez, Removal of quinolone antibiotics from wastewaters by sorption and biological degradation in laboratory-scale membrane bioreactors, Sci. Total Environ. 442 (2013) 317–328.
[29] H. Zhang, Y. Jia, S.K. Khanal, S.H. Lu, H. Fang, Q. Zhao, Understanding the role of extracellular polymeric substances on ciprofloxacin adsorption in aerobic sludge, anaerobic sludge, and sulfate-reducing Bacteria sludge systems, Environ. Sci. Technol. 52 (2018) 6476–6486.
[30] B. Yan, C.H. Niu, J. Wang, Kinetics, electron-donor-acceptor interactions, and site energy distribution analyses of norfloxacin adsorption on pretreated barley straw, Chem. Eng. J. 330 (2017) 1211–1221.
[31] Y. Jia, S.K. Khanal, H. Shu, H. Zhang, G.H. Chen, H. Lu, Ciprofloxacin degradation in anaerobic sulfate-reducing bacteria (SRB) sludge system: mechanism and pathways, Water Res. 136 (2018) 64–74.
[32] L. Zhao, X. Cao, O. Mašek, A. Zimmerman, Heterogeneity of biochar properties as a function of feedstock sources and production temperatures, J. Hazard. Mater. 256–257 (2013) 1–9.
[33] L.J. Gibson, The hierarchical structure and mechanics of plant materials, J. R. Soc. Interface 9 (2012) 2749–2766.
[34] H. Liang, K.E. DeMeester, C.-W. Hou, M.A. Parent, J.L. Caplan, C.L. Grimes, Metabolic labelling of the carbohydrate core in bacterial peptidoglycan and its applications, Nat. Commun. 8 (2017) 15015.
[35] J.G. Shang, X. Kong, L.L. He, W.H. Li, Q.J.H. Liao, Low-cost biochar derived from herbal residue: characterization and application for ciprofloxacin adsorption, Int. J. Environ. Sci. Technol. 13 (2016) 2449–2458.
[36] Y.Y. Sun, H. Li, G.C. Li, B.Y. Gao, Q.Y. Yue, X.B. Li, Characterization and ciprofloxacin adsorption properties of activated carbons prepared from biomass wastes by H_3PO_4 activation, Bioresour. Technol. 217 (2016) 239–244.
[37] Z.W. Zeng, X.F. Tan, Y.G. Liu, S.R. Tian, G.M. Zeng, L.H. Jiang, S.B. Liu, J. Li, N. Liu, Z. Yin, Comprehensive adsorption studies of doxycycline and ciprofloxacin antibiotics by biochars prepared at different temperatures, Front. Chem. 6 (2018) 80.
[38] C. Peiris, S.R. Gunatilake, T.E. Mlsna, D. Mohan, M. Vithanage, Biochar based removal of antibiotic sulfonamides and tetracyclines in aquatic environments: a critical review, Bioresour. Technol. 246 (2017) 150–159.
[39] Y. Wang, X. Wang, X. Wang, M. Liu, L. Yang, Z. Wu, S. Xia, J. Zhao, Adsorption of Pb(II) in aqueous solutions by bamboo charcoal modified with $KMnO_4$ via microwave irradiation, Colloid Surf. A 414 (2012) 1–8.
[40] M. Jouiad, N. Al-Nofeli, N. Khalifa, F. Benyettou, L.F. Yousef, Characteristics of slow pyrolysis biochars produced from Rhodes grass and fronds of edible date palm, J. Anal. Appl. Pyrol. 111 (2015) 183–190.
[41] L. Jiang, Y. Liu, G. Zeng, F. Xiao, X. Hu, X. Hu, et al., Removal of 17β-estradiol by few-layered graphene oxide nanosheets from aqueous solutions: external influence and adsorption mechanism, Chem. Eng. J. 284 (2016) 93–102.
[42] B. Yan, C.H. Niu, J. Wang, Kinetics, electron-donor-acceptor interactions, and site energy distribution analyses of norfloxacin adsorption on pretreated barley straw, Chem. Eng. J. 330 (2017) 1211–1221.
[43] X. Peng, F. Hu, J. Huang, Y. Wang, H. Dai, Z. Liu, Preparation of a graphitic ordered mesoporous carbon and its application in sorption of ciprofloxacin: kinetics, isotherm, adsorption mechanisms studies, Microporous Mesoporous Mater. 228 (2016) 196–206.
[44] M. Kowalski, K. Kowalska, J. Wiszniowski, J. Turek-Szytow, Qualitative analysis of activated sludge using FT-IR technique, Chem. Pap. 72 (2018) 2699–2706.
[45] H. Zhang, Y. Jia, S.K. Khanal, H. Lu, H. Fang, Q. Zhao, Understanding the role of extracellular polymeric substances on ciprofloxacin adsorption in aerobic sludge, anaerobic sludge, and sulfate-reducing Bacteria sludge systems, Environ. Sci. Technol. 52 (2018) 6476–6486.
[46] E.M.C.C. Batista, J. Shultz, T.T.S. Matos, M.R. Fornari, T.M. Ferreira, B. Szpoganicz, R.A. de Freitas, A.S. Mangrich, Effect of surface and porosity of biochar on water holding capacity aiming indirectly at preservation of the Amazon biome, Sci. Rep. U. K. 8 (2018) 10677.
[47] Z. Yang, R. Xing, W. Zhou, Adsorption of ciprofloxacin and Cu2+ onto biochars in the presence of dissolved organic matter derived from animal manure, Environ. Sci. Pollut. Res. 26 (2019) 14382–14392.
[48] D. Huang, X. Wang, C. Zhang, G. Zeng, Z. Peng, J. Zhou, Sorptive removal of ionizable antibiotic sulfamethazine from aqueous solution by graphene oxide-coated biochar nanocomposites: influencing factors and mechanism, Chemosphere 186 (2017) 414–421.
[49] W. Zhang, P. Yang, P. Xia, S. Xu, Y. Liu, F. Liu, D. Wang, Dynamic variation in physicochemical properties of activated sludge floc from different WWTPs and its influence on sludge dewaterability and settleability, Colloid. Surface. A 467 (2015) 124–134.
[50] N. Tixier, G. Guibaud, M. Baudu, Effect of pH and ionic environment changes on interparticle interactions affecting activated sludge flocs: a rheological approach, Environ. Technol. 24 (2003) 971–978.
[51] C. He, A. Giannis, J.-Y. Wang, Conversion of sewage sludge to clean solid fuel using hydrothermal carbonization: hydrochar fuel characteristics and combustion behavior, Appl. Energy 111 (2013) 257–266.
[52] F. Polesel, K. Lehnberg, W. Dott, S. Trapp, K.V. Thomas, B.G. Plosz, Factors influencing sorption of ciprofloxacin onto activated sludge: experimental assessment and modelling implications, Chemosphere 119 (2015) 105–111.
[53] Y. Dai, N. Zhang, C. Xing, Q. Cui, Q. Sun, The adsorption, regeneration and engineering applications of biochar for removal organic pollutants: a review, Chemosphere 223 (2019) 12–27.